Computers and Concrete, *Vol. 25, No. 3* (*2020*) *255-266*
DOI: https://doi.org/10.12989/cac.2020.25.3.255

Seismic analysis of Roller Compacted Concrete (RCC) dams considering effect of viscous boundary conditions

Muhammet Karabulut[1] and Murat E. Kartal*[2]

[1]Department of Civil Engineering, Zonguldak Bulent Ecevit University, Zonguldak, Turkey
[2]Engineering Faculty, Izmir Democracy University, Izmir, Turkey

(*Received November 8, 2018, Revised January 5, 2020, Accepted March 3, 2020*)

Abstract. This study presents comparation of fixed and viscos boundary condition effects on three-dimensional earthquake response and performance of a RCC dam considering linear and non-linear response. For this purpose, Cine RCC dam constructed in Aydın, Turkey, is selected in applications. The Drucker-Prager material model is considered for concrete and foundation rock in the nonlinear time-history analyses. Besides, hydrodynamic effect was considered in linear and non-linear dynamic analyses for both conditions. The hydrodynamic pressure of the reservoir water is modeled with the fluid finite elements based on the Lagrangian approach. The contact-target element pairs were used to model the dam-foundation-reservoir interaction system. The interface between dam and foundation is modeled with welded contact for both fixed and viscos boundary conditions. The displacements and principle stress components obtained from the linear and non-linear analyses are compared each other for empty and full reservoir cases. Seismic performance analyses considering demand-capacity ratio criteria were also performed for each case. According to numerical analyses, the total displacements and besides seismic performance of the dam increase by the effect of the viscous boundary conditions. Besides, hydrodynamic pressure obviously decreases the performance of the dam.

Keywords: demand-capacity ratio; performance analysis; roller compacted concrete (RCC) dam; viscos boundary conditions

1. Introduction

Human being always needs a source of water for drinking, cleaning, farming, livestock breeding, irrigation, electricity and other essential things from the oldest to the present. People have tried to settle around water resources and chose to live those places. However, the human population is growing at a very high level in the modern world, and therefore people need to build dams every day. Then large dams were started to be built. Civil engineers developed dams with technological measurement devices, experiments and modern computer software with new construction techniques. Nowadays, it can be seen many types of dams and continue to increase all over the world.

Roller compacted concrete dams are also constructed in accordance with the construction techniques of traditional concrete structures. However, concrete design and construction techniques are different in RCC dams. These techniques have some advantages such as rapid placement and economically benefits for construction. RCC dams are more impermeable than other dam types. Vibratory rollers, dozers and other heavy equipment are used in RCC dams' constructions. RCC related construction procedures require special attention to design and application of water tightness and seepage control, horizontal and transverse connections, facing elements and appurtenant structures (Kartal 2012). Wang *et al*. (2015) investigated the seismic performance of concrete gravity dams considering both dam reservoir and foundation interaction. They did this according to both linear and nonlinear analysis methods. In the research, they used the demand capacity ratio, cumulative overstress stress duration to determine stress and cracks. According to the linear dynamic analysis, it tends to cause a larger overstressed region and a longer cumulative overstress duration. In addition, non-linear damage-plastic analysis indicates that a ground motion can lead to larger and more dangerous cracks.

The mechanical properties of the RCC dams are performed in conventional concrete dams (USACE 1995). Engineers do not want any leakage problem from upstream face to downstream side. Therefore, the researchers have analyzed the thermal cracking problems due to these cracks and can lead to undesirable conditions Karabulut and Kartal (2019) focused on the effect of galleries on the earthquake behavior of dams to obtain more realistic results. Therefore, a roller compacted concrete (RCC) dam with and without galleries are examined under ground motion effects. According to numerical analyses, the effect of galleries is clear on the response of RCC dam. Lin *et al*. (2014) investigated seismic performance of Shapai roller-compacted concrete (RCC) arch dam and Zipingpu concrete-faced rockfill (CFR) dam using Wenchuan earthquake (Mw=8.0). Zhang and Wang (2013) studied nonlinear dynamic response of a concrete gravity dam considering near-field and far-fault ground motion influences. Ghaedi *et al.* (2015) focused on the seismic analysis of roller compacted concrete (RCC) dams

*Corresponding author, Professor
E-mail: murat.kartal@idu.edu.tr

http://www.techno-press.org/?journal=cac&subpage=8
ISSN: 1598-8198 (Print), 1598-818X (Online)

considering effect of sizes and shapes of galleries. Ghaedi *et al.* (2015) studied the change of gallery sizes and shapes under seismic effects.

Monteiro and Barros (2008) studied the combination of the static self-weight and hydrostatic pressure of level of full storage with the seismic activities associated with scaled design accelerogram. They presented the change of accelerations, displacements and stresses during earthquake. Yazdani and Alembagheri (2017) investigated nonlinear dynamic response of a gravity dam considering near-fault ground motion. They took into account the full reservoir condition in nonlinear time-history analyzes. Liu *et al.* (2015) focused on real-time construction quality monitoring of storehouse surfaces for RCC dams. They studied quality of construction is in roller compacted concrete (RCC) dams. Zhang *et al*. (2009) investigated relocating mesh method for the calculation of temperature field of RCC dam. They studied error and feasibility of the relocating mesh method. Considering the results, the method has less memory and less software run time, high calculation precision. Alembagheri and Ghaemian (2013) studied the damage evaluation of a concrete arch dam. They used nonlinear incremental seismic analysis in the study. The dam-foundation interaction effects have been investigated by varying foundation's and concrete's modulus of elasticities. Yilmazturk *et al.* (2015) focused on seismic assessment of a monolithic RCC gravity dam. They modeled three-dimensional dam-foundation-reservoir interaction in this study. According to results, the necessity and importance of a full 3D analyses for such systems were underlined by comparing the results with two dimensional analyses. Lotfi (2004) investigated direct frequency domain analysis of concrete arch dams based on FE-(FE-HE)-BE technique. A FE-(FE-HE)-BE procedure is presented for dynamic analysis of concrete arch dams. Furthermore, the effects of canyon shape on response of dam, was also discussed. Türker and Bayraktar (2014) studied vibration-based damage identification of concrete arch dams. The paper aims to show the effectiveness of the model updating method for global damage detection on a laboratory arch dam model. Sevim and Altunisik (2014) investigated construction stages analyses using time dependent material properties of concrete arch dams. In this study a double curvature Type-5 arch dam suggested in Arch Dams symposium in England in 1968 is selected as a numerical example. Santillán *et al*. (2015) studied thermal behavior of concrete dams during operation. It is clear that thermal effects are significant loads for assessing concrete dam behaviour during operation. Therefore, in this paper proposes the use of a new one-dimensional model based on an explicit finite difference scheme which is improved by means of the reported methodology for computing the heat fluxes through the dam faces. Altunisik and Sesli (2015) investigated dynamic response of concrete gravity dams using different water modelling approaches: Westergaard, Lagrange and Euler. For this purpose, Sariyar concrete gravity dam located on the Sakarya River is selected as a case study. Akkose (2016) focused on nonlinear seismic response of arch dams. It is investigated that arrival direction effects of travelling waves on non-linear seismic response of arch dams. It is seen that the seismic waves might reach on the dam site from any direction. Altunisik *et al*. (2018) studied validated prototype model of an arch dam which is one of five arch dam types suggested at the "Arch Dams" Symposium in England in 1968. It is clear that there is a good agreement between all results obtained by similarity requirements with scaling laws and enlarged finite element models in this study. Kartal and Karabulut (2018) studied performance of a RCC dam considering materially non-linearity. In this study, they suggested that all analyses may be renewed for viscous or non-reflecting boundary conditions. It may result safer results for the response and performance of the dam. Khanzaei *et al.* (2015) studied thermal and structural response of roller compacted concrete (RCC) dams. The results show that the used boundary and initial conditions provide realistic responses from the numerical models. Also, an increase in the tensile stresses was observed after five years of dam completion. However, the locations and distribution shapes are mostly similar. Ghaedi *et al.* (2017) investigated flexible foundation effect on seismic analysis of roller compacted concrete (RCC) dams. Finite Element Method is used in this study. The difference between rigid and flexible foundation conditions has been revealed.

Earthquakes can affect big water structures, dams and can damage significantly. The aim of this study is to investigate the effect of different boundary conditions on the stress and displacement of the dam during a strong ground motion. Besides, it is also intended to obtain seismic performance of the roller compacted concrete dam. In this study, Cine RCC dam was modeled by finite element method with ANSYS software. Material properties were obtained from experimental data of the dam. Three-dimensional finite element dam model was considered for fixed and viscos conditions. The Cine RCC dam were evaluated for eight different cases under Loma Prieta earthquake records.

Each case results were compared with each other. Comparing all case results give an information about viscos and fixed boundaries condition effects on an RCC dam. It can be observed serious differences between principle stress results according to linear and non-linear time history analysis in these cases. All dynamic analyses were performed under 1989 Loma Prieta earthquake records. The horizontal displacements, principle tensile and compressive stresses for viscos and fixed conditions were compared with each other. Besides, the most critical point in dam body was investigated by performance analysis for linear and nonlinear analysis. After the performance analysis, Demand/Capacity (D/C) and principle stresses graphics were obtained from numerical analyses for eight cases at the most critical location in the upstream side of the dam. Moreover, using the D/C-principle stresses graphics, the cumulative inelastic duration and demand-capacity (D/C) ratio graphs can be determined. It should be taken into account the safety and damaging of Cine dam if it hits under this kind of seismic motion using demand capacity ratio graphs. Because the graphics indicate that whether the allowable stress limits are exceeded or not.

2. Formulation of Dam-Foundation-Reservoir Interaction by the Lagrangian Approach

The fluid system formulation based on the Lagrangian approach was used by Wilson and Khalvati (1983) as following. In this approach, fluid is assumed to be linearly compressible, inviscid and irrotational. For a general three-dimensional fluid, pressure-volumetric strain relationships can be written in matrix form as follows

$$\begin{Bmatrix} P \\ P_x \\ P_y \\ P_z \end{Bmatrix} = \begin{bmatrix} C_{11} & 0 & 0 & 0 \\ 0 & C_{22} & 0 & 0 \\ 0 & 0 & C_{33} & 0 \\ 0 & 0 & 0 & C_{44} \end{bmatrix} \begin{Bmatrix} \varepsilon_v \\ w_x \\ w_y \\ w_z \end{Bmatrix} \tag{1}$$

where P, C_{11}, and ε_v are the pressures which are equal to mean stresses, the bulk modulus and the volumetric strains of the fluid, respectively. Since irrationality of the fluid is considered (Bathe 1996) like penalty methods, rotations and constraint parameters are included in the pressure-volumetric strain equation (Eq. (1)) of the fluid. In this equation P_x, P_y, P_z, is the rotational stress; C_{22}, C_{33}, C_{44} are the is the constraint parameters and w_x, w_y and w_z are the rotations about the Cartesian axes x, y and z.

In this study, the equations of motion of the fluid system are obtained using energy principles. Using the finite element approximation, the total strain energy of the fluid system may be written as

$$\pi_e = \frac{1}{2} \mathbf{U}_f^{\,T} \mathbf{K}_f \mathbf{U}_f \tag{2}$$

where U_f and K_f are the nodal displacement vector and the stiffness matrix of the fluid system, respectively. K_f is obtained by the sum of the stiffness matrices of the fluid elements as follows

$$\left.\begin{aligned} \mathbf{K}_f &= \sum \mathbf{K}_f^e \\ \mathbf{K}_f^e &= \int_V \mathbf{B}_f^{e\,T} \mathbf{C}_f \mathbf{B}_f^e \mathrm{d}V^e \end{aligned}\right\} \tag{3}$$

where C_f is the elasticity matrix consisting of diagonal terms in Eq. (1) $\mathbf{B}_f^e$ is the strain-displacement matrix of the fluid elements.

An important behavior of fluid systems is the ability to displace without a change in volume. For reservoir and storage tanks, this movement is known as sloshing waves in which the displacement is in the vertical direction. The increase in the potential energy of the system because of the free surface motion can be written as

$$\pi_S = \frac{1}{2} \mathbf{U}_{sf}^T \mathbf{S}_f \mathbf{U}_{sf} \tag{4}$$

where U_{sf} and S_f are the vertical nodal displacement vector and the stiffness matrix of the free surface of the fluid system, respectively. S_f is obtained by the sum of the stiffness matrices of the free surface fluid elements as follows

$$\left.\begin{aligned} \mathbf{S}_f &= \sum \mathbf{S}_f^e \\ \mathbf{S}_f^e &= \rho_f g \int_{\mathbf{A}} \mathbf{h}_s^T \mathbf{h}_s \mathrm{d}A^e \end{aligned}\right\} \tag{5}$$

where h_s is the vector consisting of interpolation functions of the free surface fluid element. ρ_f and g are the mass density of the fluid and the acceleration due to gravity, respectively. Besides, kinetic energy of the system can be written as

$$\mathrm{T} = \frac{1}{2} \dot{\mathbf{U}}_f^T \mathbf{M}_f \dot{\mathbf{U}}_f \tag{6}$$

where $\dot{\mathbf{U}}_f$ and M_f are the nodal velocity vector and the mass matrix of the fluid system, respectively. M_f is also obtained by the sum of the mass matrices of the fluid elements as follows

$$\left.\begin{aligned} \mathbf{M}_f &= \sum \mathbf{M}_f^e \\ \mathbf{M}_f^e &= \rho_f \int_V \mathbf{H}^T \mathbf{H} \mathrm{d}V^e \end{aligned}\right\} \tag{7}$$

where H is the matrix consisting of interpolation functions of the fluid element. if (Eq. (2), (4) and (6)) are combined using the Lagrange's equation (Clough and Penzien 1993); the following set of equations is obtained

$$\mathbf{M}_f \ddot{\mathbf{U}}_f + \mathbf{K}_f^* \mathbf{U}_f = \mathbf{R}_f \tag{8}$$

where $\mathbf{K}_f^*$, $\ddot{\mathbf{U}}_f$, $\mathbf{U}_f$ and $\mathbf{R}_f$ are the system stiffness matrix including the free surface stiffness, the nodal acceleration and displacement vectors and time-varying nodal force vector for the fluid system, respectively. In the formation of the fluid element matrices, reduced integration orders (Wilson and Khalvati 1983).

The equations of motion of the fluid system, (Eq. (8)), have a similar form with those of the structure system. To obtain the coupled equations of the fluid-structure system, the determination of the interface condition is required. Since the fluid is assumed to be inviscid, only the displacement in the normal direction to the interface is continuous at the interface of the system. Akkas *et al.* (1979) assumed that the structure has the positive face and the fluid has the negative face, the boundary condition at the fluid-structure interface is

$$U_n^- = U_n^+ \tag{9}$$

where U_n is the normal component of the interface displacement. Using the interface condition, the equation of motion of the coupled system to ground motion including damping effects are given by

$$\mathbf{M_c}\ddot{\mathbf{U}}_\mathbf{c} + \mathbf{C_c}\dot{\mathbf{U}}_\mathbf{c} + \mathbf{K_c}\mathbf{U_c} = \mathbf{R_c} \tag{10}$$

in which $\mathbf{M_c}$, $\mathbf{C_c}$, and $\mathbf{K_c}$ are the mass, damping and stiffness matrices for the coupled system, respectively. $\mathbf{U_c}$, $\dot{\mathbf{U}}_\mathbf{c}$, $\ddot{\mathbf{U}}_\mathbf{c}$ and $\mathbf{R_c}$ are the vectors of the displacements, velocities, accelerations and external loads of the coupled system, respectively.

3. The Drucker-Prager model

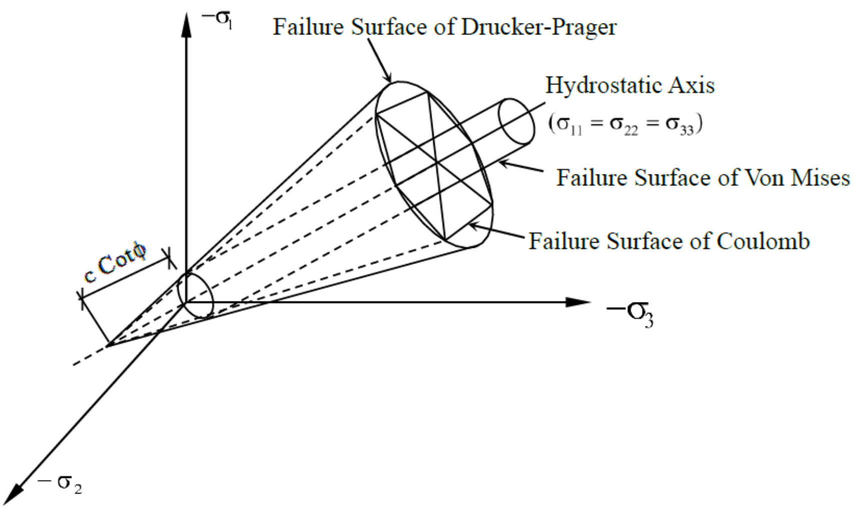

Fig. 1 Failure criteria for Coulomb, Drucker-Prager and von Mises used by Chen and Mizuno (1990)

There are many criteria for determination of yield surface or yield function of materials. The Drucker-Prager criterion is widely used for frictional materials such as rock and concrete. Drucker and Prager (1952) obtained a convenient yield function to determine elasto-plastic behavior of concrete smoothing Mohr-Coulomb criterion (Fig. 1). This function is defined (Chen and Mizuno 1990) as

$$f = \alpha I_1 + \sqrt{J_2 - k} \tag{11}$$

where α and k are constants which depend on cohesion (c) and angle of internal friction (ϕ) of the material given by

$$\alpha = \frac{2\ Sin\varphi}{\sqrt{3}\,(3 - Sin\varphi)} \qquad k = \frac{6c\ Cos\varphi}{\sqrt{3}\,(3 - Sin\varphi)} \tag{12}$$

In Eq. (11), I1 is the first invariant of stress tensor (σ_{ij}) formulated as follows

$$I_1 = \sigma_{11} + \sigma_{22} + \sigma_{33} \tag{13}$$

and J_2 is the second invariant of deviatoric stress tensor (s_{ij}) given by

$$J_2 = \frac{1}{2} s_{ij}\, s_{ij} \tag{14}$$

where, s_{ij} is the deviatoric stresses as yielded below.

$$s_{ij} = \sigma_{ij} - \delta_{ij}\sigma_m \qquad (i, j = 1,2,3) \tag{15}$$

In Eq. (15), δ_{ij} is the kronecker delta, which is equal to 1 for $i=j$; 0 for $i \neq j$, and σ_m is the mean stress and obtained as follows

$$\sigma_m = \frac{I_1}{3} = \frac{\sigma_{ii}}{3} \tag{16}$$

If the terms in Eq. (15) are obtained by Eq. (16) and replaced in Eq. (14), the second invariant of the deviatoric stress tensor can be obtained as follows

$$J_2 = \frac{1}{6}\left[(\sigma_{11} - \sigma_{22})^2 + (\sigma_{22} - \sigma_{33})^2 + (\sigma_{33} - \sigma_{11})^2\right] + \sigma_{12}^{\ 2} + \sigma_{13}^{\ 2} + \sigma_{23}^{\ 2} \tag{17}$$

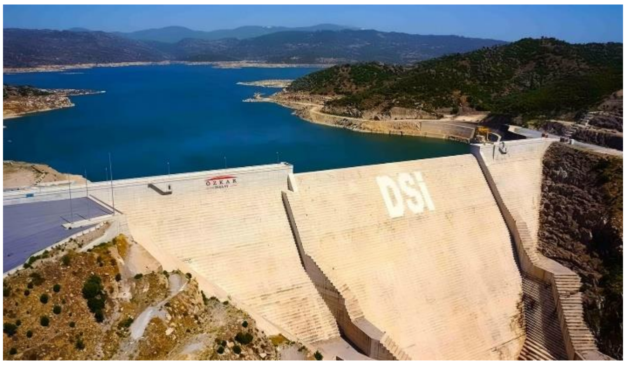

Fig. 2 The general view of Cine RCC dam (DSI 2018)

4. Description and modeling of Cine RCC dam

4.1 Cine dam

Cine dam, located approximately 16 km southeast of Cine, Aydın, was constructed in 2010 by General Directorate of State Hydraulic Works (Fig. 2). It was established on Cine River. This dam was projected as a roller compacted concrete dam. Its reservoir is used for irrigation and energy purposes. The dam crest is 372.5 m in length and 9 m in wide. The maximum height and base width of the dam are 136.5 m and 142.5 m, respectively. The maximum height of the reservoir water is considered as 98.77 m. The annual total power generation capacity is 118 GW.

4.2 Material properties of Cine RCC dam

The three-dimensional finite element model of Cine dam is modelled considering two layered foundation with gneiss rock. Material properties of Cine roller compacted concrete dam body and foundation are given in Table 1. The cohesion for the concrete used in an RCC dam changes from 0.5 MPa to 4.1 MPa (Luhr 2000). The tensile strength and the compressive strength of the concrete used in the dam body are 1.3 MPa and 20 MPa, respectively (DSI, 2012).

Table 1 Material properties of Cine dam

	Material Properties					
	Modulus of elasticity (MPa)	Poisson's ratio	Mass density (kg/m^3)	Cohesion (kPa)	Angel of internal friction	Angel of dilatation
Concrete (Dam Body)	2.50E4	0.2	2500	900	41	11
Blocky gneiss (foundation)	1.75E4	0.15	2400	4000	39	9
Very blocky gneiss (valley)	1.4E4	0.15	2400	3000	38	8

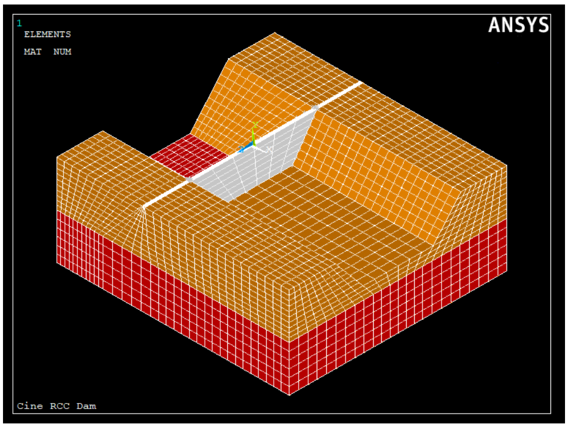

Fig. 3 Finite element model of Cine dam for empty reservoir condition

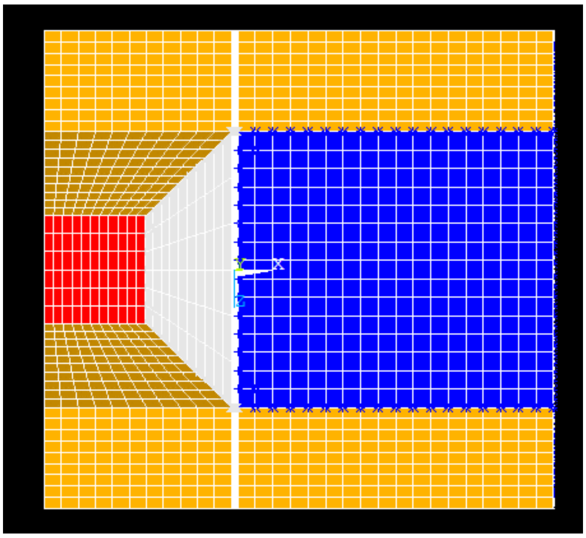

Fig. 4 Finite element model of Cine dam for full reservoir condition

4.3 Finite element model of Cine cam

This study considers three-dimensional finite element model (FEM) of Cine RCC dam with fixed and viscos boundary conditions (Figs. 3 and 4). In this model, if the height of the dam is indicated as '*H*', the foundation rock is extended as '*H*' in the downstream river direction and gravity direction. Besides, foundation rock and reservoir water model is extended as "3*H*" in the upstream direction. Fluid and solid element matrices are computed using the

Table 2 Case properties

Case Numbers	Reservoir	Boundary	Connection	Analysis Type
Case 1	Empty	Fixed	Welded	Linear
Case 2				Non-linear
Case 3	Full			Linear
Case 4				Non-linear
Case 5	Empty	Viscos	Welded	Linear
Case 6				Non-linear
Case 7	Full			Linear
Case 8				Non-linear

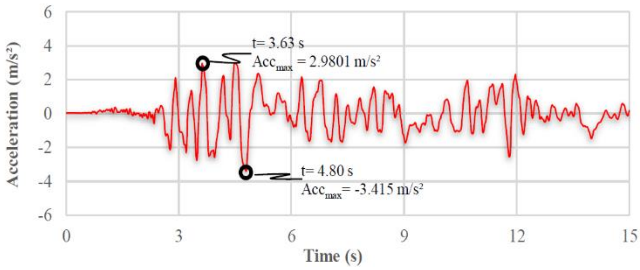

(a) East-West direction

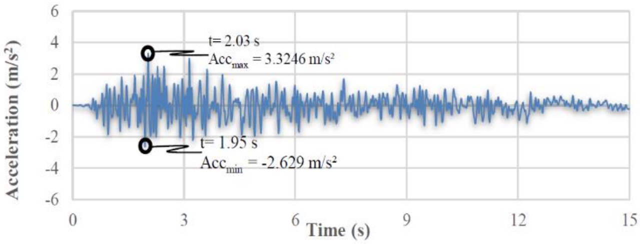

(b) North-South direction

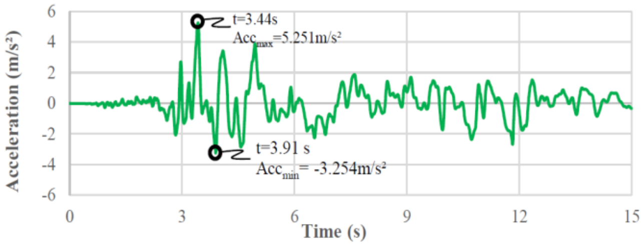

(c) Vertical direction

Fig. 5 The Loma Prieta 1989 Earthquake accelerograms

Gauss numerical integration technique. SOLID 45 elements were used to modelling dam body, foundation and valley part of Cine dam. Besides, reservoir water modelled by Lagrangian Approach using FLUID 80 elements.

In this study, the RCC dam were modelled with and without water to observe the effect of hydrodynamic on the earthquake behavior of the dam. The three-dimensional finite element model of Cine RCC dam is obtained using finite element method by ANSYS software. Maximum principle tensile and compressive stresses were determined for the bottom point of upstream side of dam body.

4.4 Numerical analysis cases

Four different cases were investigated in the scope of this study. Different analysis cases for reservoir conditions were presented in Table 2. The aim of these cases is to reveal the effect of the hydrodynamic pressure and non-linear response of the dam separately.

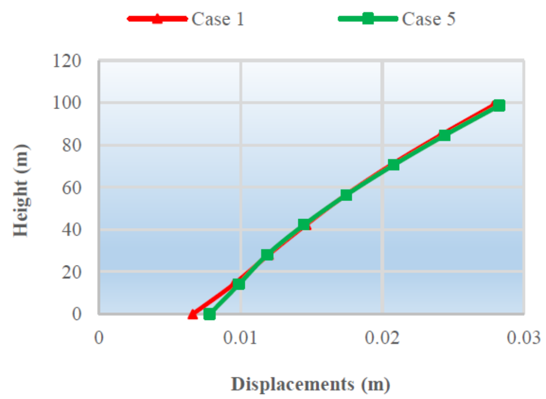

(a) Case 1 and Case 5

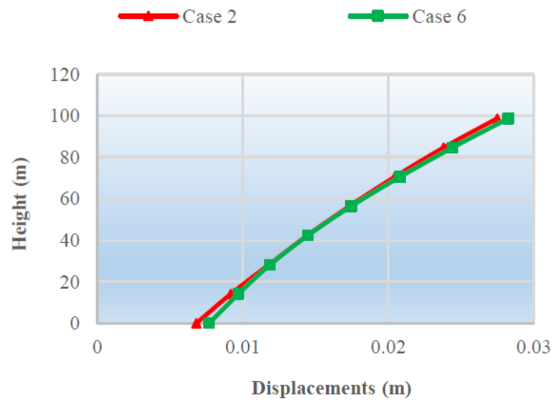

(b) Case 2 and Case 6

Fig. 6 Maximum displacements by height for empty reservoir condition

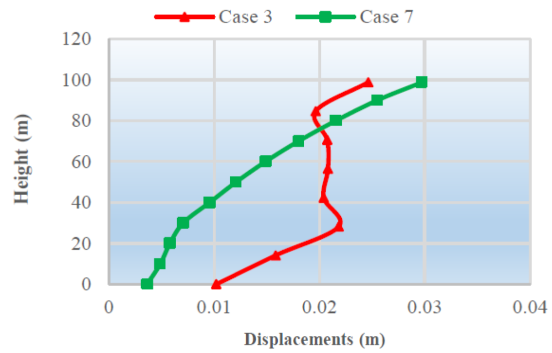

(a) Case 3 and Case 7

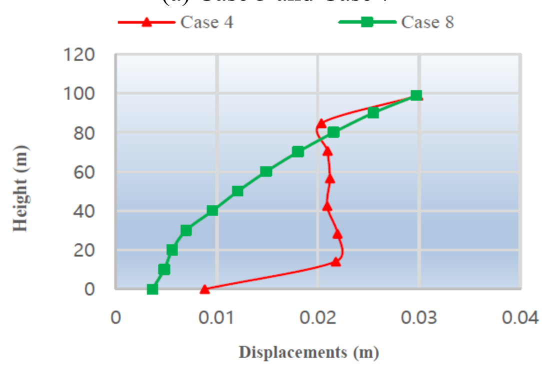

(b) Case 4 and Case 8

Fig. 7 Maximum displacements by height for full reservoir condition

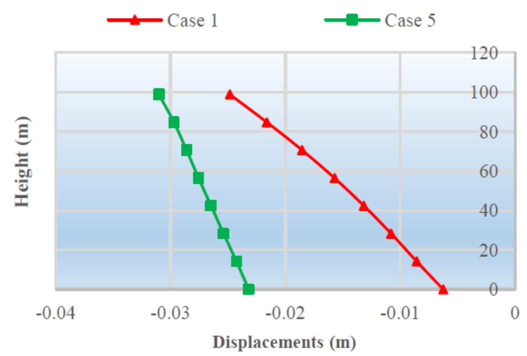

(a) Case 1 and Case 5

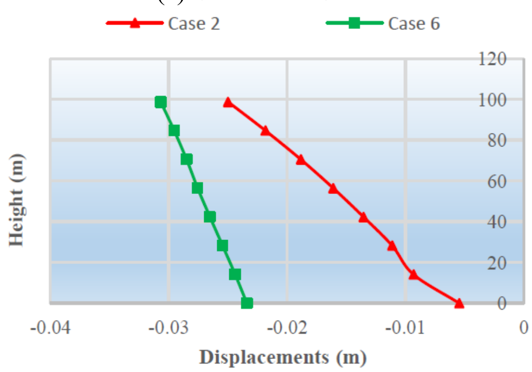

(b) Case 2 and Case 6

Fig. 8 Minimum displacements by height for empty reservoir condition

4.5 Loma Prieta 1989 Earthquake records

An earthquake severely shaked San Francisco and Monterey Bay regions at 5:04:15 p.m. on October 17, 1989. Epicenter point is 37.04° north latitude and 121.88° west longitude near Loma Prieta peak in the Santa Cruz Mountains. The depth of the earthquake is 18 km and extended 35 km along the fault. John *et al*. (1999) determined the earthquake moment magnitude is 7.1 Md. In this study, east-west, north-south and vertical components of earthquake were used. The accelerograms of the earthquake are given in Fig. 5. The earthquake duration time is 15 seconds and sampling interval is 0.01 second in the earthquake analyses.

5. Numerical analysis and results

The Cine RCC dam was investigated for two different boundary conditions. First one is fixed boundary condition and second is viscos. The effects of fixed and viscous boundary conditions on dam behavior and performance are presented in this study. Maximum-minimum displacements and principle tensile and compressive stress components during earthquake throughout dam body height are investigated.

5.1 Displacements

The maximum horizontal displacements are examined for upstream and downstream directions. Figs. 6-9 give the

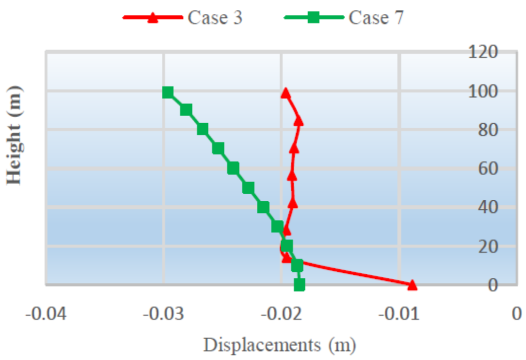

(a) Case 3 and Case 7

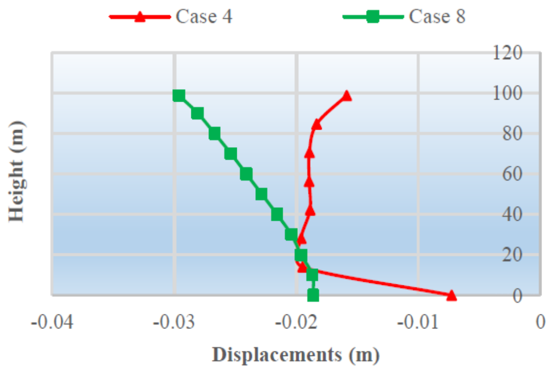

(b) Case 4 and Case 8

Fig. 9 Minimum displacements by height for full reservoir condition

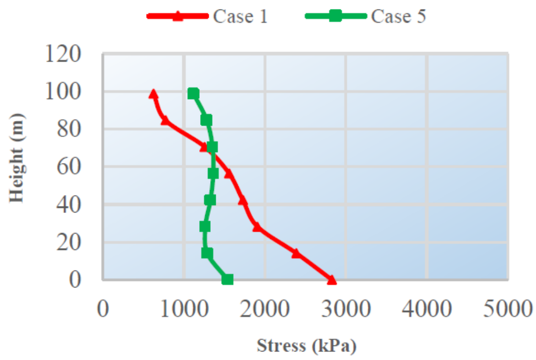

(a) Case 1 and Case 5

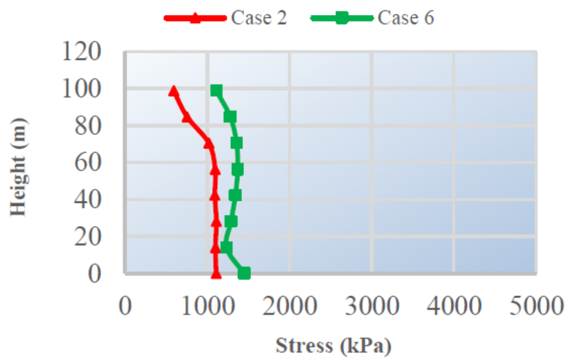

(b) Case 2 and Case 6

Fig. 10 Maximum tensile stresses by height for empty reservoir condition

change of horizontal displacements by dam height according to fixed and viscos boundary conditions for empty and full reservoir conditions considering linear and nonlinear response.

The maximum horizontal displacements due to viscos boundary conditions are greater than those for fixed boundary conditions according to both linear and nonlinear analyses in downstream side. Generally, the maximum displacements in downstream side are close to each other by height for empty reservoir case due to each boundary conditions in linear and nonlinear analyses.

The maximum displacements by height in downstream side resemble each other in full reservoir cases for linear and nonlinear analyses and the same boundary condition. However, the change of those are different for fixed and viscos boundary conditions. The horizontal displacements by height are usually greater for fixed boundary conditions. However, displacements increase by hydrodynamic pressure.

Moreover, the horizontal displacements in empty reservoir case for viscos boundary condition are greater than those for fixed boundary conditions according to linear and nonlinear analyses in the upstream side. The horizontal displacements by height for full reservoir case in nonlinear analyses are obviously higher than those in linear analyses due to fixed boundary condition. The change of the maximum displacements is smoother and continuous in viscos boundary condition as compared to fixed boundary condition.

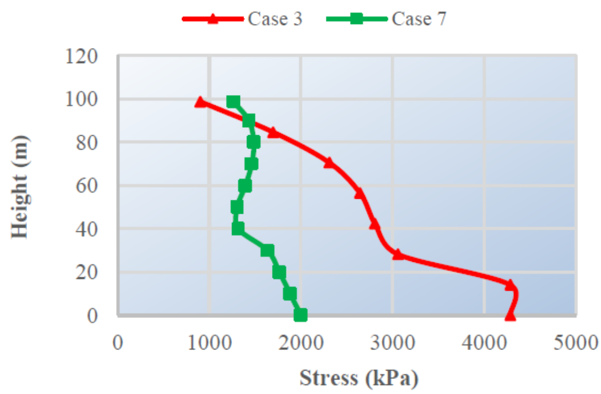

(a) Case 3 and Case 7

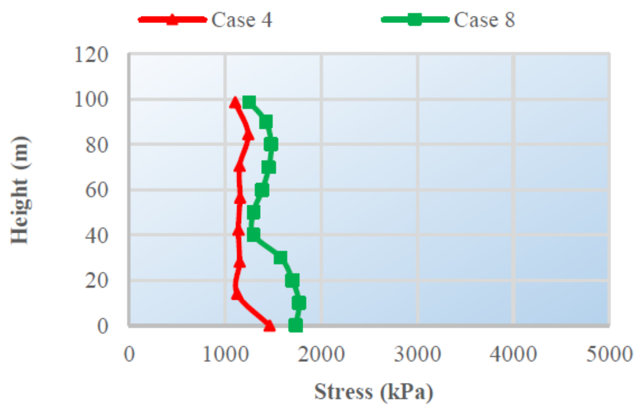

(b) Case 4 and Case 8

Fig. 11 Maximum tensile stresses by height for full reservoir condition

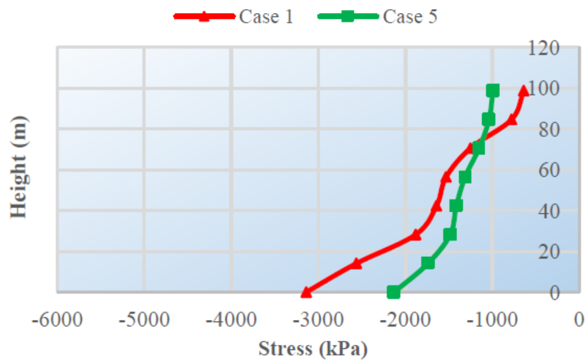

(a) Case 1 and Case 5

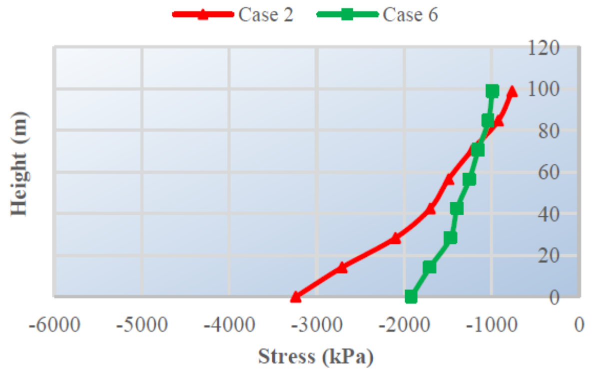

(b) Case 2 and Case 6

Fig. 12 Maximum compressive stresses by height for empty reservoir condition

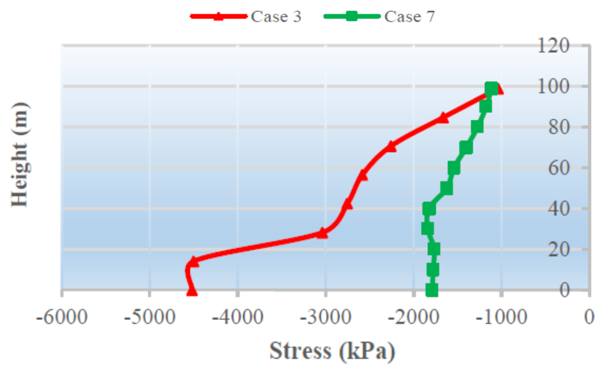

(a) Case 3 and Case 7

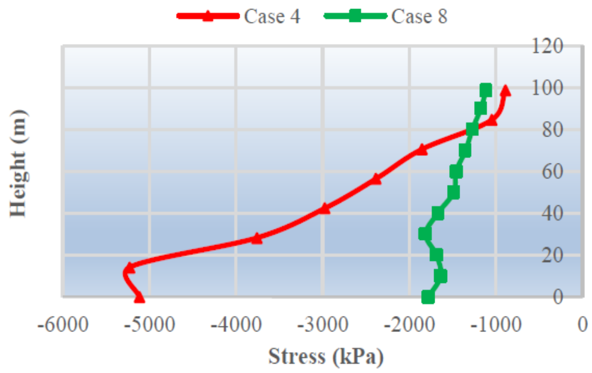

(b) Case 4 and Case 8

Fig. 13 Maximum compressive stresses by height for empty reservoir condition

5.1 Stresses

The maximum principle tensile and compressive stresses occurred in dam body examined for viscos and fixed boundary conditions. Figs. 10-13 give the change of maximum principle stress components by dam height according to empty and full reservoir cases for linear and nonlinear analyses results.

The maximum principle tensile stresses are greater for viscos boundary conditions in empty reservoir cases as compared to fixed boundary conditions according to nonlinear analyses. However, while these stresses are higher at crest according to linear analyses for viscos boundary conditions, those are greater at the base of the dam for fixed boundary conditions. The maximum principle tensile stresses clearly increase by hydrodynamic pressure in all linear and nonlinear analyses. Besides, the principle tensile stresses are lower in nonlinear analyses for each boundary and reservoir cases as compared to those in linear analyses.

The maximum principle compressive stresses in both reservoir cases are obtained lower for viscos boundary conditions as compared to fixed boundary conditions. On the other hand, the principle compressive stresses obtained from nonlinear analyses are greater than those in linear analyses for fixed boundary conditions. The hydrodynamic pressure increases the principle compressive stresses for each boundary conditions in linear and nonlinear analyses.

6. Results of performance analysis

This section of the study describes a systematic approach for evaluation of the seismic performance and potential of damage using linear and nonlinear time-history analyses. Magnitudes of stress changing by time and cumulative inelastic duration of stresses were considered to explain the potential damage level. The level of probable damage is considered acceptable if the results from the linear elastic time history analyses fall below a specified threshold expressed in terms of cumulative inelastic duration and demand-capacity ratios. Otherwise the damage is considered severe requiring nonlinear methods of analyses (Ghanaat 2002). According to linear dynamic analyses, it was observed that the tensile stress occurred in concrete exceed many times the threshold values for all boundary and reservoir conditions. This case requires nonlinear dynamic analyses of Cine RCC dam under earthquake accelerograms. In such cases, the realistic seismic performance can only be determined for nonlinear response during earthquake. Therefore, all the linear analyses carried out for different boundary and reservoir conditions were also realized considering nonlinear response of the dam. Thereby, more reliable seismic performance dam under various conditions were determined.

6.1 Demand-capacity ratios (DCR) and cumulative inelastic duration

The demand-capacity ratios for CFR dams are defined as the ratio of the computed principal tensile stresses to

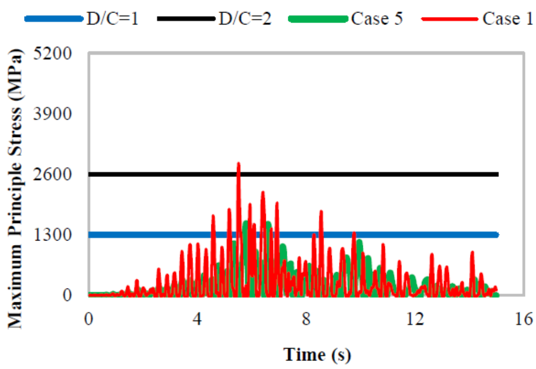

(a) Case 1 and Case 5

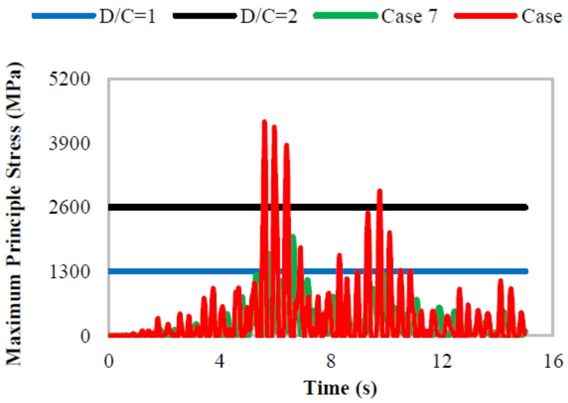

(b) Case 3 and Case 7

Fig. 14 Maximum principle stresses during earthquake for linear analyses

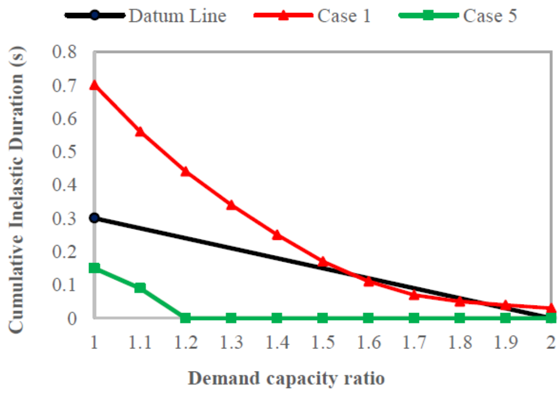

(a) Case 1 and Case 5

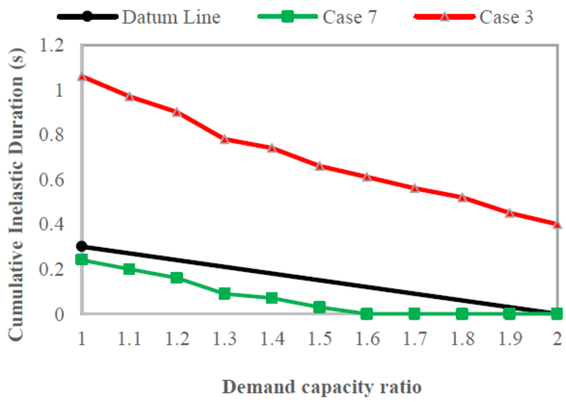

(b) Case 3 and Case 7

Fig. 15 Performance analysis according to linear solutions

tensile strength of the concrete. As discussed previously demand-capacity ratio is limited to 2.0, thus permitting stresses up to twice the static or at the level of dynamic apparent tensile strength of the concrete, as long as the overstressed region is less than 15% of the dam surface area. The cumulative duration beyond a certain level of demand-capacity ratio is obtained by multiplying number of stress values exceeding that level of tensile strength by the time-step of the time-history analysis. The cumulative duration refers to the total duration of all stress excursions beyond a certain level of demand-capacity ratio. Although tensile strength of concrete is affected by the rate of seismic loading, the acceptance criteria employ stable tensile strength in computation of the demand-capacity ratios. The reason for this is to account for the lower strength of the lift lines and provide some level of conservatism in estimation of damage using the results of linear elastic analysis.

The demand-capacity ratio (DCR) for gravity and RCC dams is defined as the ratio of the calculated principal stress to tensile strength of the concrete. The tensile strength of the plain concrete used in calculation of DCR is gathered from the uni-axial splitting tension tests or from

$$ft = 1.7f'c^{\frac{2}{3}} \tag{18}$$

proposed by Raphael (1984), where f_c' is the compressive strength of the concrete.

Cumulative inelastic duration may be gathered roughly by multiplying number of stress points over an accurate stress range by numeric time history analysis. The higher cumulative duration, the higher the possibilities for more damage. For RCC dams a lower cumulative duration of 0.3 is assumed, mainly because RCC dams resist loads by cantilever mechanism only, as opposed to arch dams that rely on both the arch and cantilever actions (U.S. Army Corps of Engineers 2016).

6.2 Performance criteria for RCC dams

The seismic performance of RCC dams is evaluated on the basis of load combination cases, demand capacity ratios, and the related cumulative duration. The performance is formulated for the maximum design earthquake (MDE). The MDE is identified as the maximum range of earthquake for which a structure is designed (U.S. Army Corps of Engineers 2016). Three performance levels are considered:

Small or not damaging: Response of dam is considered to be within the linear elastic range of behavior with little or no possibility of damage if the calculated demand-capacity ratios are less than or equal to 1 (*D/C*=1)

Acceptable damage level: The dam will exhibit nonlinear response in the form of cracking and joint opening if the computed demand-capacity ratios exceed 1.0. The level of nonlinear response or cracking is considered acceptable if stress demand-capacity ratios are less than 2.0 (*D/C*=2).

Severe damage: The damage is considered severe when demand-capacity ratios are greater than 2.0 (*D/C*=2). In these situations, a nonlinear time-history analysis may be

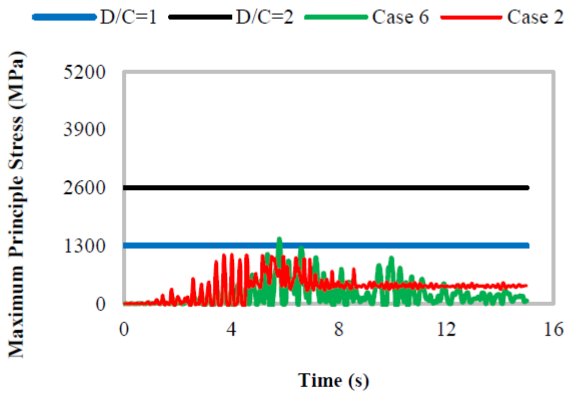

(a) Case 2 and Case 6

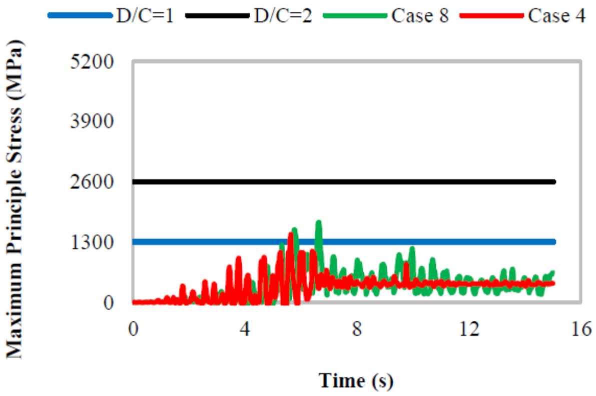

(b) Case 4 and Case 8

Fig. 16 Maximum principle stresses during earthquake for nonlinear analyses

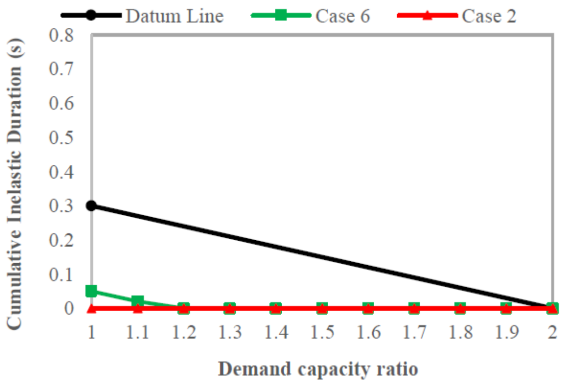

(a) Case 2 and Case 6

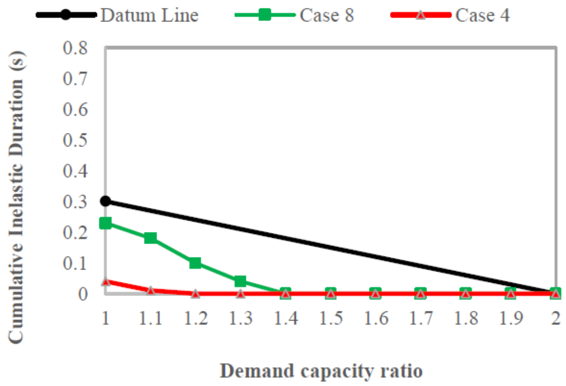

(b) Case 4 and Case 8

Fig. 17 Performance analysis according to nonlinear solutions

required to assess the damage and thus the performance more accurately.

According to numeric time-history analyses, principle stress-time graphs are drawn and they show how many times the stress value exceed the threshold in Figs. 14-16. Demand capacity ratio-cumulative inelastic duration graphs consist of principle stress and time components. The demand capacity ratio graphics should be examined in Fig. 15 for making a realistic comment on Cine RCC dam. When the Fig. 14 is checked, stresses seem as too high if compared the acceptable limit (datum line) in linear analyses. It shows that nonlinear analyses necessary to obtain more realistic results. After that, nonlinear time history analyses are completed and the results of them are given in Fig. 15. Huge differences can be seen between linear and nonlinear demand capacity ratios in Fig. 15. It is clear that in Fig. 16, there is no stress value over the threshold in nonlinear analysis for empty and full reservoir conditions and these display smaller stresses than linear analyses.

Moreover, the more important and deductive cases are Case 3-4 and Case7-8 due to their full reservoir properties. Full reservoir condition and evaluation of its hydrodynamic effect on dam should carefully be examined. Because of that, linear and nonlinear analyses for full reservoir condition were also analyzed. According to linear analysis, it can be easily seen that reservoir effect is considerably obvious on principle stresses in Fig. 14(b) when it is compares with Fig. 14(a) and Fig. 14(b). Besides, the most important case is Case 8 in this study due to the fact that it includes full reservoir nonlinear analysis and also viscos boundary condition. Results of Case 8 have much more importance for dam safety criteria. Principle stresses gathered from Case 8 are given Fig. 16(b). When Fig. 16(a) and (b) are compared, nonlinearity appears with reduced stresses in Fig. 16(b).

7. Conclusions

In this study, finite element analyses of Cine RCC dam was performed using three-dimensional finite element model considering viscos and fixed boundary conditions. Besides, hydrodynamic pressure of reservoir water was taken into consideration by Lagrangian Approach. The Drucker-Prager material model was used in nonlinear time-history analyses in finite element analyses. Loma Prieta 1989 earthquake acceleration records used in numerical dynamic analyses. The earthquake response of Cine RCC dam and evaluation of seismic performance have been compared each other for both fixed and viscos boundary conditions. First of all, dam behaviour was examined under strong ground motion effect. For this purpose, linear and nonlinear time-history analyses considering empty and full reservoir conditions were carried out. The tensile-compressive stresses and horizontal displacements are compared in all cases. Then, performance analysis of Cine

RCC dam for both boundary conditions were performed.

According to numerical analysis some important results are deducted from this study as follows.

- The maximum and minimum displacements are greater for viscous boundary conditions.
- The maximum and minimum displacements clearly increase by the hydrodynamic pressure effect of the reservoir water for each boundary conditions.
- While the principle tensile stresses decrease in nonlinear analyses, the principle compressive stresses increase and this increase is obvious for fixed boundary conditions.

According to performance analysis the situation of the dam after earthquake is studied to determine as follows.

- Linear solutions indicate that nonlinear analyses should be carried out to obtain realistic seismic performance of the dam for both empty and full reservoir conditions. Furthermore, dam performance clearly decreases for fixed boundary in full reservoir condition.
- The performance is adequate for viscos boundary condition in both reservoir condition.
- The performance is sufficient for all nonlinear analyses.

References

Akkas, N., Akay, H.U. and Yilmaz, Ç. (1979), "Applicability of general-purpose finite element programs in solid-fluid interaction problems", *Comput. Struct.*, **10**, 773-783. https://doi.org/10.1016/0045-7949(79)90041-5.

Akkose, M. (2016), "Arrival direction effects of travelling waves on nonlinear seismic response of arch dams", *Comput. Concrete*, **18**(2), 179-199. https://doi.org/10.12989/cac.2016.18.2.179.

Alembagheri, M. and Ghaemian, M. (2013), "Damage assessment of a concrete arch dam through nonlinear incremental dynamic analysis", *Rock Found. Dyn. Earthq. Eng.*, **44**, 127-137. https://doi.org/10.1016/j.soildyn.2012.09.010.

Altunisik, C.A. and Sesli, H. (2015), "Dynamic response of concrete gravity dams using different water modelling approaches: Westergaard, Lagrange and Euler", *Comput. Concrete*, **16**(3), 429-448. https://doi.org/10.12989/cac.2015.16.3.429.

Altunisik, C.A., Kalkan, E. and Basagi, H. (2018), "Structural behavior of arch dams considering experimentally validated prototype model using similitude and scaling laws", *Comput. Concrete*, **22**(2), 101-116. https://doi.org/10.12989/cac.2018.22.1.101.

Bathe K. J. (1996), *Finite Element Procedures*, 1037.

Chen, W.F. and Mizuno, E. (1990), *Nonlinear Analysis in Rock foundation Mechanics-Theory and Implementation*,

Clough, R. and Penzien, J. (1993), *Dynamics of Structures*.

Drucker, C. and Prager, W. (1952), "Rock foundation mechanics and plastic analysis of limit design", *Q. Appl. Math.*, **10**, 157-165.

DSI (2012), General Directorate of State Hydraulic Works, The XXI, Regional Directorate, Aydın, Turkey.

DSI (2018), General Directorate of State Hydraulic Works. http://www.dsi.gov.tr/dsi-galeri/barajlar/Turkey.

Ghaedi, K., Hejazi, F., Zainah, I. and Khanzaei, P. (2017), "Flexible foundation effect on seismic analysis of Roller Compacted Concrete (RCC) dams using finite element method", *KSCE J. Civil Eng.*, **22**(4), 1275-1287. https://doi.org/10.1007/s12205-017-1088-6.

Ghaedi, K., Jameel, M., Ibrahim, Z. and Khanzaei, P. (2015), "Seismic analysis of roller compacted concrete (RCC) dams considering effect of sizes and shapes of galleries", *KSCE J. Civil Eng.*, **20**, 261-272. https://doi.org/10.1007/s12205-015-0538-2.

Ghanaat, Y. (2002), "Seismic Performance and Damage Criteria for Concrete Dams", *Third US-Japan Work. Adv. Res. Earthq. Eng. Dams*, 1-15.

Karabulut, M. and Kartal, E.M. (2019), "Earthquake response of roller compacted concrete dams including galleries", *Struct. Eng. Mech.*, **72**(2), 141-153. https://doi.org/10.12989/sem.2019.72.2.141 141.

Kartal, E.M. and Karabulut, M. (2018), "Earthquake performance evaluation of three-dimensional roller compacted concrete dams", *Earthq. Struct.*, **14**(2), 167-178. https://doi.org/10.12989/eas.2018.14.2.167.

Kartal, M.E. (2012), "Three-dimensional earthquake analysis of roller-compacted concrete dams", *Nat. Hazard. Earthq. Syst.*, **12**, 2369-2388. https://doi.org/10.5194/nhess-12-2369-2012.

Khanzaei, P., Abdulrazeg, A.A., Samali, B. and Ghaedi, K. (2015), "Thermal and structural response of RCC dams during their service life", *J. Therm. Stress.*, **38**, 591-609. https://doi.org/10.1080/01495739.2015.1015862.

Lin, P., Huang, B., Li, Q, Wang, R. (2014), "Hazard and seismic reinforcement analysis for typical large dams following the Wenchuan earthquake", *Eng. Geol.*, **194**, 86-97. https://doi.org/10.1016/j.enggeo.2014.05.011.

Liu, Y., Zhong, D., Cui, B., Zhong, G. and Wei, Y. (2015), "Study on real-time construction quality monitoring of storehouse surfaces for RCC dams", *Automat Constr.*, **49**, 100-112. https://doi.org/10.1016/j.autcon.2014.10.003.

Lotfi, V. (2004), "Direct frequency domain analysis of concrete arch dams based on FE-(FE-HE)-BE technique", *Comput. Concrete*, **1**(3), 285-302. https://doi.org/10.12989/cac.2004.1.3.285.

Luhr, D.R. (2000), "Engineering and design roller-compacted concrete", USACE., Washington.

Monteiro, G. and Barros, R.C. (2008), "Seismic analysis of a roller compacted concrete gravity dam in Portugal", *The 14th World Conference on Earthquake Engineering*, Beijing, October.

Nakata, J.K., Meyer, C.E., Wilshire, H.G., Tinsley, J.C., Updegrove, W.S., Peterson, D.M., ... & Diggles, M.F. (1999), "U.S. Geological Survey", Charles G. Groat, Director. https://pubs.usgs.gov/dds/dds-29/.

Raphael, J.M. (1984), "Tensile strength of concrete", *J. Proc.*, **81**, 158-165.

Santillán, D., Salete, E., Toledo, M.A. and Granados, A. (2015), "An improved 1D-model for computing the thermal behaviour of concrete dams during operation. Comparison with other approaches", *Comput. Concrete*, **15**(1), 103-126. https://doi.org/10.12989/cac.2015.15.1.103.

Sevim, B. and Altunisik, C.A. (2014), "Construction stages analyses using time dependent material properties of concrete arch dams", *Comput. Concrete*, **14**(5), 599-612. http://dx.doi.org/10.12989/cac.2014.14.5.599.

Türker, T. and Bayraktar, A. (2014), "Vibration based damage identification of concrete arch dams by finite element model updating", *Comput. Concrete*, **13**(2), 209-220. http://dx.doi.org/10.12989/cac.2014.13.2.209.

U.S. Army Corps of Engineers (1995), Gravity Dam Design, USACE Eng Man., 88.

U.S. Army Corps of Engineers (2016), "Earthquake design and evaluation for civil works projects", *USACE*, **2**, 1110-1806.

Wang, G., Wang, Y., Lu, W., Zhou, W. and Zhou, C. (2015), "Integrated duration effects on seismic performance of concrete gravity dams using linear and nonlinear evaluation methods", *Rock Found. Dyn. Earthq. Eng.*, **79**, 223-236.

https://doi.org/10.1016/j.soildyn.2015.09.020.
Wilson, E.L. and Khalvati, M. (1983), "Finite elements for the dynamic analysis of fluid-solid systems", *Int. J. Numer. Meth. Eng*., **19**, 1657-1668. https://doi.org/10.1002/nme.1620191105.
Yazdani, Y. and Alembagheri, M. (2017), "Nonlinear seismic response of a gravity dam under near-fault ground motions and equivalent pulses", *Rock Found. Dyn. Earthq. Eng*., **92**, 621-632. https://doi.org/10.1016/j.soildyn.2016.11.003.
Yilmazturk, S.M., Arici, Y. and Binici, B. (2015), "Seismic assessment of a monolithic RCC gravity dam including three dimensional dam-foundation-reservoir interaction", *Eng. Struct*., **100**, 137-148. https://doi.org/10.1016/j.engstruct.2015.05.041.
Zhang, S. and Wang, G. (2013), "Effects of near-fault and far-fault ground motions on nonlinear", *Rock Found. Dyn. Earthq. Eng*., **53**, 217-229.
Zhang, X.F., Li, S.Y., Chen, Y.L. and Chai, J.R. (2009), "The development and verification of relocating mesh method for the computation of temperature field of RCC dam", *Adv. Eng. Softw*., **40**, 1119-1123. https://doi.org/10.1016/j.advengsoft.2009.05.006.

CC

Notations

ρ:	density of water
ρ_r:	reservoir bottom material
C:	wave speeds for the material on the reservoir bottom
C_r:	wave speeds for the material on the reservoir side
P:	stress
C_{11}:	bulk modulus
$\boldsymbol{\varepsilon_v}$:	volumetric strains of the fluid
$\boldsymbol{U_f}$:	nodal displacement vector
$\boldsymbol{K_f}$:	stiffness matrix of the fluid system
C_f:	elasticity matrix consisting of diagonal terms
k:	constants which depend angle of internal friction
$\boldsymbol{B_f}$:	strain-displacement matrix of the fluid element
$\boldsymbol{S_f}$:	stiffness matrix of the free surface of the fluid system
$\boldsymbol{\dot{U}_f}$:	nodal velocity vector
$\boldsymbol{M_f}$:	mass matrix of the fluid system
$\boldsymbol{H}$:	matrix consisting of interpolation functions of the fluid element
$\boldsymbol{U_n}$:	normal component of the interface displacement
$\boldsymbol{M_c}$:	mass for the coupled system
$\boldsymbol{C_c}$:	damping for the coupled system
$\boldsymbol{K_c}$:	stiffness matrices for the coupled system
α:	constants which depend on cohesion
$\boldsymbol{S}_{\mathbf{ij}}$:	the deviatoric stresses